Available online at www.sciencedirect.com
SCIENCE DIRECT®
Journal of Computational Physics 189 (2003) 45–62
JOURNAL OF COMPUTATIONAL PHYSICS
www.elsevier.com/locate/jcp

Finite element modelling of free surface flows on inclined and curved beds

M. Quecedo [a,b], M. Pastor [b,c,*]

[a] ENUSA, Madrid, Spain
[b] Grupo M^2i, Department of Applied Mathematics, ETSI de Caminos, Madrid, Spain
[c] Centro de Estudios y Experimentación de Obras Públicas, Alfonso XII 3, 28014 Madrid, Spain

Received 8 March 2002; received in revised form 17 February 2003; accepted 18 February 2003

Abstract

The solution of gravity-driven free surface flows typically resorts to the Shallow Water Equations, SWE. In turn, the derivation of the SWE incorporates a number of assumptions and within them, it should be stressed that of quasi-horizontal fluid velocities. However, when the flow occurs onto a steep and curved topography, the velocities are parallel to the bed rather than horizontal and curvature effects may affect the fluid flow. This paper extends the SWE incorporating the inclined and curved bed effects thus, allowing the analysis of gravity flows on actual topographies. Due to the similarity between the generalized and the standard SWE, the numerical methods available for the solution of the SWE can be easily applied for the solution of the generalized equations. Within these methods, this paper uses the Taylor–Galerkin algorithm. The results obtained in the numerical test cases indicate that incorporating the slope and curvature effects in the model is relevant for granular flows and of reduced effect in the remaining cases.

1. Introduction

The classical approach to solve gravity-driven free surface flows such as flood waves, mudflows, debris flows, etc. is based on the assumption that the fluid depth is smaller than a representative dimension of the extension of the fluid spill. This assumption allows the complex Navier–Stokes 3-D problem, involving in addition the calculation of the evolution of the surface separating the fluid from the air, to be collapsed in the vertical direction and solved them as a 2-D problem: the shallow water problem. Although methods are available to solve a Navier–Stokes problem involving two fluids with a high density ratio, such as those presented in [8,10], the 2-D approach saves significant computational effort and allows performing calculations involving realistic domains. Besides, numerical methods to solve the Shallow Water Equations abound, see for instance [1,2,12,18].

* Corresponding author.
E-mail address: manuel.pastor@cedex.es (M. Pastor).

0021-9991/03/$ - see front matter
doi:10.1016/S0021-9991(03)00200-6

The derivation of the Shallow Water Equations, SWE, starts from the assumption of reduced fluid depth. The derivation uses a Cartesian coordinate system where the vertical direction is oriented in the direction of the gravity. Thus, the gravity is considered approximately perpendicular to the free surface and to the bed. Therefore, bed slopes should be small and the velocities quasi-horizontal.

These requirements are fulfilled when the gravity current runs onto quasi-horizontal areas. However, when it runs onto steep slopes and curved beds, the fluid velocities are parallel to the bed rather than horizontal. In some cases, this issue can be mitigated by considering the XY plane parallel to the average slope. Unfortunately, this approach is not feasible when the spill of fluid runs onto slopes with opposite sign: a run-up flow.

In addition to this slope effect, the bed curvature incorporates into the momentum conservation equations a centrifugal force, proportional to the curvature times the velocity squared, which it is not considered in the SWE.

This issue is solved by some authors by directly incorporating the centrifugal forces into the momentum conservation equation as external forces in the global $\{X, Y\}$ reference system, see for instance [4,5].

Savage and Hutter have derived [15,17] a 1-D system of equations incorporating the slope and curvature effects. In this 1-D case, the issue of the reference system is greatly simplified as the principal curvature directions are fixed and known a priori.

Recently, Gray et al. [7] extended the Savage and Hutter formulation to complex geometries. In this approach, the actual basal topography is modelled by defining a mean topography allowing a simple orthogonal curvilinear reference system and, then, superposing a shallow basal topography on it. This mean reference surface is not unique and various choices are possible. Besides, the superposed topography must be shallow respective to the specified reference surface.

This paper presents the derivation of 2-D depth integrated equations using a curvilinear system of reference which incorporates the effects of the bed slope and curvature thus, avoiding the aforementioned issues, and applicable to a generic topography. Considering a curvilinear reference system corresponding to the principal curvature directions in each point of the basal surface, the resulting equations are greatly simplified and formally equivalent to the SWE. Therefore, the Taylor–Galerkin scheme already used by the authors [9] to solve dam break problems including drying–wetting areas within the FEM context is used to solve the generalized system of equations. Finally, the performance of the proposed Generalized Shallow Water Equations is shown by comparison against the corresponding SWE results calculated considering different fluid rheologies.

2. Mathematical model

The flow of a gravity-driven free surface flow is typically described using depth integrated equations. These equations are obtained from the Navier–Stokes equations particularized for an incompressible fluid

$$\rho \frac{\partial \bar{U}}{\partial t} + \rho \mathrm{div}\left(\bar{U} \circledast \bar{U}\right) = \mathrm{div}\,\boldsymbol{\tau} - \mathrm{grad}\, p + \rho \bar{b}, \tag{1}$$

$$\mathrm{div}\,\bar{U} = 0, \tag{2}$$

where

- ρ is the fluid density,
- $\bar{U}$ is the 3-D velocity vector,
- $\boldsymbol{\tau}$ is the viscous stress tensor,
- p is the pressure, and $\bar{b}$ is the vector of body forces: Coriolis and gravity.

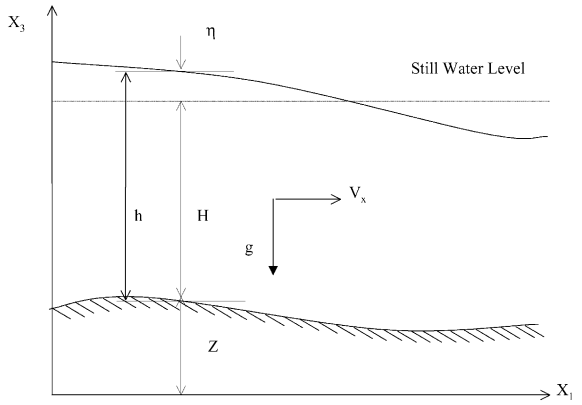

Fig. 1. Shallow Water Equations notation.

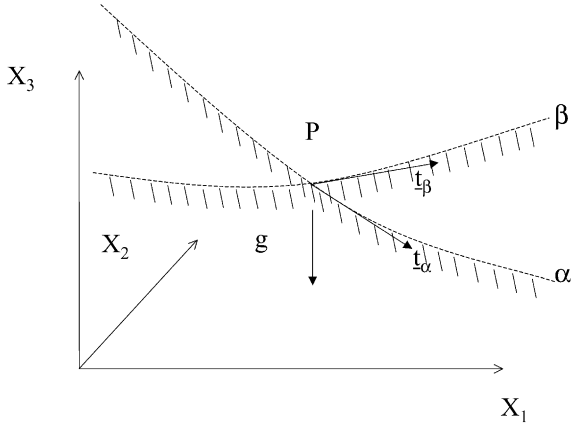

Fig. 2. Curvilinear reference system used to describe the basal surface.

Considering a Cartesian reference system, see Fig. 1 for a 2-D presentation, where X_3 is oriented in the vertical direction, coincident with the gravity force, and assuming quasi-horizontal velocities, the integration of the Navier–Stokes equations along the depth results in the Shallow Water Equations, SWE, see texts books such as [1,3] for the details of the derivation.

However, in the case of shallow flows on steep slopes, the flow velocities are parallel to the bed rather than horizontal, as considered in the SWE, and the slope changes, i.e., the curvature effects need to be incorporated into the governing equations. In this case, a curvilinear coordinate system is necessary to describe the flow.

Fig. 2 presents the curvilinear reference system $\{\alpha, \beta\}$ proposed to describe the basal surface. To simplify the expressions of the differential operators in this reference system, the α and β coordinate lines correspond to the principal curvature directions of the bed surface in each point. Thus, the corresponding natural vectors $\{\bar{t}_\alpha, \bar{t}_\beta\}$ are orthogonal. This reference system changes respective to a Cartesian system $\{X_i\}$ along the basal surface.

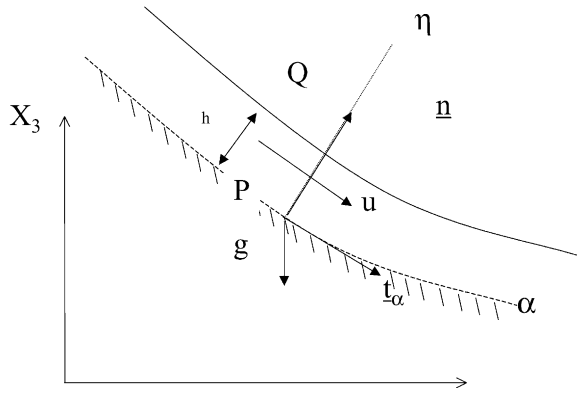

Fig. 3. Coordinate system used along the fluid depth. Cut along the α coordinate line.

A third coordinate, η, see Fig. 3, is used to describe the spatial position in the normal direction to the bed surface. Considering that the flow depth is small compared to the length and width of the fluid spill and smaller than the minimum radius of curvature, a point located within the fluid can be described as, see Fig. 3,

$$\bar{x} = \bar{x}_P(\alpha, \beta) + \eta \bar{n}, \tag{3}$$

which particularizes to a point Q at the free surface as

$$\bar{x}_Q = \bar{x}_P(\alpha, \beta) + h \bar{n}.$$

Using this geometrical description, the governing equations are obtained by

1. writing the Navier–Stokes and the normal velocity at the free surface equations in the curvilinear coordinate system described in Figs. 2 and 3;
2. deriving dimensionless equations to resolve the higher order terms;
3. depth integration of the dimensionless equation, neglecting the higher order terms;
4. recovering dimensions to get the final governing equations.

The following sections describes each step in this sequence.

2.1. Navier–Stokes equations in the curvilinear coordinates system

Eq. (1) assumes that the total stress tensor, $\boldsymbol{\sigma}$, comprises a viscous component, $\boldsymbol{\tau}$, which is a function of rate of deformation tensor, $\mathbf{D}$, plus an isotropic component, $-p\mathbf{1}$, existing at the fluid at rest [11]

$$\boldsymbol{\sigma} = -p\mathbf{1} + \boldsymbol{\tau}. \tag{4}$$

For generality, the following derivation does not considered any stress decomposition. The specialization to different types of fluid is done at the end of the derivation.

Continuity equation. The continuity equation (2) is written in terms of the velocity components, u^i, and curvilinear coordinates, ξ^i, as

$$\frac{1}{|\bar{h}_i|}\frac{\partial u^i}{\partial \xi^i} + u^j \frac{\partial \bar{e}_j}{\partial \xi^i} \cdot \bar{h}^i = 0, \quad i, j = 1, 2, 3,$$

where

- $\bar{h}_i = \partial\bar{x}/\partial\xi_i$,
- $\bar{h}^i \cdot \bar{h}_j = \delta^i_j$,
- $\bar{e}_j = \frac{\bar{h}_j}{|\bar{h}_j|}$.

Considering now Eq. (3) to obtain the natural vectors, $\bar{h}_i$, the continuity equation may be written as

$$(1-\chi_\beta\eta)\frac{\partial u}{\partial\alpha} + (1-\chi_\alpha\eta)\frac{\partial v}{\partial\beta} + \frac{\partial}{\partial\eta}\left[(1-\chi_\alpha\eta)(1-\chi_\beta\eta)w\right] = 0, \tag{5}$$

where

- $\{u, v, w\}$ are the components of the velocity in the $\{\alpha, \beta, \eta\}$ reference system and,
- χ_α, χ_β are the curvatures in the α and β directions, respectively.

Momentum equations. Considering that the only body force, $\bar{b}$, is the gravity

$$\bar{b} = -g\bar{k},$$

where $\bar{k}$ is the unit vector in the X_3 direction, i.e., neglecting the Coriolis forces, the three components of the momentum equation are

- Component α

$$\begin{aligned}
&\rho\left\{\frac{\partial}{\partial t}\left[(1-\chi_\alpha\eta)(1-\chi_\beta\eta)u\right] + (1-\chi_\beta\eta)\frac{\partial u^2}{\partial\alpha} + \frac{\partial}{\partial\eta}\left[(1-\chi_\alpha\eta)(1-\chi_\beta\eta)uw\right]\right.\\
&\quad\left. - \chi_\alpha(1-\chi_\beta\eta)uw + (1-\chi_\alpha\eta)\frac{\partial(uv)}{\partial\beta}\right\}\\
&= (1-\chi_\beta\eta)\frac{\partial\sigma^\alpha}{\partial\alpha} + (1-\chi_\alpha\eta)\frac{\partial\sigma^{\alpha\beta}}{\partial\beta} + (1-\chi_\beta\eta)\frac{\partial(1-\chi_\alpha\eta)\sigma^{\alpha\eta}}{\partial\eta}\\
&\quad - \left[(1-\chi_\beta\eta)\chi_\alpha + (1-\chi_\alpha\eta)\chi_\beta\right]\sigma^{\alpha\eta} - (1-\chi_\alpha\eta)(1-\chi_\beta\eta)\rho g\bar{k}\cdot\bar{t}_\alpha.
\end{aligned} \tag{6}$$

- Component β

$$\begin{aligned}
&\rho\left\{\frac{\partial}{\partial t}\left[(1-\chi_\alpha\eta)(1-\chi_\beta\eta)v\right] + (1-\chi_\beta\eta)\frac{\partial(uv)}{\partial\alpha} + \frac{\partial}{\partial\eta}\left[(1-\chi_\alpha\eta)(1-\chi_\beta\eta)vw\right]\right.\\
&\quad\left. - \chi_\beta(1-\chi_\beta\eta)vw + (1-\chi_\alpha\eta)\frac{\partial(v^2)}{\partial\beta}\right\}\\
&= (1-\chi_\beta\eta)\frac{\partial\sigma^{\alpha\beta}}{\partial\alpha} + (1-\chi_\alpha\eta)\frac{\partial\sigma^\beta}{\partial\beta} + \frac{\partial}{\partial\eta}\left[(1-\chi_\alpha\eta)(1-\chi_\beta\eta)\sigma^{\beta\eta}\right]\\
&\quad - \left[(1-\chi_\beta\eta)\chi_\alpha + (1-\chi_\alpha\eta)\chi_\beta\right]\sigma^{\beta\eta} - (1-\chi_\alpha\eta)(1-\chi_\beta\eta)\rho g\bar{k}\cdot\bar{t}_\beta.
\end{aligned} \tag{7}$$

- Component η

$$\begin{aligned}
&\rho\left\{\frac{\partial}{\partial t}\left[(1-\chi_\alpha\eta)(1-\chi_\beta\eta)w\right] + \chi_\alpha(1-\chi_\beta\eta)u^2 + \chi_\beta(1-\chi_\alpha\eta)v^2 + (1-\chi_\beta\eta)\frac{\partial(uw)}{\partial\alpha}\right.\\
&\quad\left. + (1-\chi_\alpha\eta)\frac{\partial(vw)}{\partial\beta} + \frac{\partial\left[(1-\chi_\alpha\eta)(1-\chi_\beta\eta)w^2\right]}{\partial\eta}\right\}\\
&= (1-\chi_\beta\eta)\frac{\partial\sigma^{\alpha\eta}}{\partial\alpha} + (1-\chi_\alpha\eta)\frac{\partial\sigma^{\beta\eta}}{\partial\beta} + (1-\chi_\alpha\eta)(1-\chi_\beta\eta)\frac{\partial\sigma^\eta}{\partial\eta} - \left[(1-\chi_\beta\eta)\chi_\alpha + (1-\chi_\alpha\eta)\chi_\beta\right]\sigma^\eta\\
&\quad + (1-\chi_\beta\eta)\chi_\alpha\sigma^\alpha + (1-\chi_\alpha\eta)\chi_\beta\sigma^\beta - (1-\chi_\alpha\eta)(1-\chi_\beta\eta)\rho g\bar{k}\cdot\bar{n}.
\end{aligned} \tag{8}$$

Free surface velocity. The velocity component normal to the free surface, w^s, is calculated from the material derivative of the depth, h, versus time as

$$w^s = \frac{\mathrm{D}h}{\mathrm{D}t} = \frac{\partial h}{\partial t} + \operatorname{grad} h \cdot \bar{u}^s,$$

which results in the following expression:

$$w^s = \frac{\partial h}{\partial t} + \frac{1}{1-\chi_\alpha h}\frac{\partial h}{\partial \alpha}u^s + \frac{1}{1-\chi_\beta h}\frac{\partial h}{\partial \beta}v^s. \tag{9}$$

2.2. Dimensionless equations

Considering now a length L characterizing the water spill in the α direction, a width W in the β direction and a characteristic depth H the following relationships between dimensioned and dimensionless variables can be defined as

$$\begin{aligned}
&u = \sqrt{gL}\hat{u}, \quad \alpha = L\hat{\alpha}, \quad \chi_\alpha = \frac{\lambda_\alpha}{L}\hat{\chi}_\alpha,\\
&v = \frac{W}{L}\sqrt{gL}\hat{v}, \quad \beta = W\hat{\beta}, \quad \chi_\beta = \frac{\lambda_\beta}{L}\hat{\chi}_\beta,\\
&w = \frac{H}{L}\sqrt{gL}\hat{w}, \quad \eta = H\hat{\eta}, \quad \boldsymbol{\sigma} = \rho g H\hat{\boldsymbol{\sigma}},\\
&t = \sqrt{\frac{L}{g}}\hat{t}, \quad \varepsilon = \frac{H}{L}, \quad \delta = \frac{W}{L},
\end{aligned} \tag{10}$$

where the ratio between a characteristic depth and length of the spill, $\varepsilon = H/L$, is assumed to be small, i.e.,

$$\varepsilon = \frac{H}{L} \ll 1. \tag{11}$$

This condition indicates that the depth of the gravity current is much smaller than the horizontal dimensions. Note that using different weighting in the α, β and η directions will result in simpler dimensionless equations with the higher order terms being a function of ε alone.

Writing Eqs. (5)–(9) in the dimensionless variables reveals the order ε, or superior, components and considering (11), these higher order terms will be neglected. However, as spatial derivatives of the stress tensor components can be large, the terms of the form $\varepsilon(\partial\sigma/\partial\xi)$are kept.

The resulting equations, where for simplicity the $\hat{}$ symbol used to identify the dimensionless variables in the previous table is dropped, are:

Continuity

$$\left(1-\chi_\beta\lambda_\beta\eta\varepsilon\right)\frac{\partial u}{\partial \alpha} + \left(1-\chi_\alpha\lambda_\alpha\eta\varepsilon\right)\frac{\partial v}{\partial \beta} + \frac{\partial}{\partial \eta}\left[\left(1-\chi_\alpha\lambda_\alpha\eta\varepsilon\right)\left(1-\chi_\beta\lambda_\beta\eta\varepsilon\right)w\right] = 0. \tag{12}$$

Momentum

- Component α

$$\begin{aligned}
&\frac{\partial}{\partial t}\left[(1-\chi_\alpha\lambda_\alpha\eta\varepsilon)(1-\chi_\beta\lambda_\beta\eta\varepsilon)u\right]+(1-\chi_\beta\lambda_\beta\eta\varepsilon)\frac{\partial u^2}{\partial\alpha}+\frac{\partial}{\partial\eta}\left[(1-\chi_\alpha\lambda_\alpha\eta\varepsilon)(1-\chi_\beta\lambda_\beta\eta\varepsilon)uw\right]\\
&\quad-\chi_\alpha\lambda_\alpha(1-\chi_\beta\lambda_\beta\eta\varepsilon)uw+(1-\chi_\alpha\lambda_\alpha\eta\varepsilon)\frac{\partial(uv)}{\partial\beta}\\
&=(1-\chi_\beta\lambda_\beta\eta\varepsilon)\varepsilon\frac{\partial\sigma^\alpha}{\partial\alpha}+(1-\chi_\alpha\lambda_\alpha\eta\varepsilon)\frac{\varepsilon}{\delta}\frac{\partial\sigma^{\alpha\beta}}{\partial\beta}+(1-\chi_\beta\lambda_\beta\eta\varepsilon)\frac{\partial(1-\chi_\alpha\lambda_\alpha\eta\varepsilon)\sigma^{\alpha\eta}}{\partial\eta}\\
&\quad-(1-\chi_\alpha\lambda_\alpha\eta\varepsilon)(1-\chi_\beta\lambda_\beta\eta\varepsilon)\bar{\boldsymbol{k}}\cdot\bar{\boldsymbol{t}}_\alpha.
\end{aligned}\tag{13}$$

- Component β

$$\begin{aligned}
&\delta\left\{\frac{\partial}{\partial t}\left[(1-\chi_\alpha\lambda_\alpha\eta\varepsilon)(1-\chi_\beta\lambda_\beta\eta\varepsilon)v\right]+(1-\chi_\beta\lambda_\beta\eta\varepsilon)\frac{\partial(uv)}{\partial\alpha}+\frac{\partial}{\partial\eta}\left[(1-\chi_\alpha\lambda_\alpha\eta\varepsilon)(1-\chi_\beta\lambda_\beta\eta\varepsilon)vw\right]\right.\\
&\quad\left.-\chi_\beta\lambda_\beta(1-\chi_\beta\eta)\varepsilon vw+(1-\chi_\alpha\lambda_\alpha\eta\varepsilon)\frac{\partial(v^2)}{\partial\beta}\right\}\\
&=(1-\chi_\beta\lambda_\beta\eta\varepsilon)\varepsilon\frac{\partial\sigma^{\alpha\beta}}{\partial\alpha}+(1-\chi_\alpha\lambda_\alpha\eta\varepsilon)\frac{\varepsilon}{\delta}\frac{\partial\sigma^\beta}{\partial\beta}+\frac{\partial}{\partial\eta}\left[(1-\chi_\alpha\lambda_\alpha\eta\varepsilon)(1-\chi_\beta\lambda_\beta\eta\varepsilon)\sigma^{\beta\eta}\right]\\
&\quad-(1-\chi_\alpha\lambda_\alpha\eta\varepsilon)(1-\chi_\beta\lambda_\beta\eta\varepsilon)\bar{\boldsymbol{k}}\cdot\bar{\boldsymbol{t}}_\beta.
\end{aligned}\tag{14}$$

- Component η

$$\begin{aligned}
\chi_\alpha\lambda_\alpha(1-\chi_\beta\lambda_\beta\eta\varepsilon)u^2+\chi_\beta\lambda_\beta(1-\chi_\alpha\lambda_\alpha\eta\varepsilon)\delta^2v^2&=(1-\chi_\alpha\lambda_\alpha\eta\varepsilon)(1-\chi_\beta\lambda_\beta\eta\varepsilon)\frac{\partial\sigma^\eta}{\partial\eta}\\
&\quad-(1-\chi_\alpha\lambda_\alpha\eta\varepsilon)(1-\chi_\beta\lambda_\beta\eta\varepsilon)\bar{\boldsymbol{k}}\cdot\bar{\boldsymbol{n}}.
\end{aligned}\tag{15}$$

Free surface velocity

$$w^s=\frac{\partial h}{\partial t}+\frac{u^s}{1-\chi_\alpha\lambda_\alpha\varepsilon h}\frac{\partial h}{\partial\alpha}+\frac{v^s}{1-\chi_\beta\lambda_\beta\varepsilon h}\frac{\partial h}{\partial\beta}.\tag{16}$$

2.3. Depth integration

Now, Eqs. (12)–(15) are integrated along the coordinate η from the bed, $\eta=0$, to the free surface, $\eta=h$. As it is a standard procedure when obtaining depth integrating equations, the Leibniz's rule is used.

Continuity equation. Integrating (12) from $\eta=0$ to $\eta=h$ and considering the kinematic condition (16) yields

$$\frac{\partial(\bar{u}h)}{\partial\alpha}+\frac{\partial(\bar{v}h)}{\partial\beta}+\frac{\partial h}{\partial t}=0+\mathrm{O}(\varepsilon),$$

where

- $\bar{u}=\frac{1}{h}\int_0^h u\,\mathrm{d}\eta$,
- $\bar{v}=\frac{1}{h}\int_0^h v\,\mathrm{d}\eta$.

Momentum equations. Integrating along the depth and neglecting terms of order $\mathrm{O}(\varepsilon)$ and higher, the components of the momentum equations may be written as

- α Momentum

$$\frac{\partial(\bar{u}h)}{\partial t}+\frac{\partial(\bar{u}^2h)}{\partial\alpha}+\frac{\partial(\bar{u}\bar{v}h)}{\partial\beta}=\varepsilon\int_0^h\frac{\partial\sigma^{\alpha}}{\partial\alpha}\,\mathrm{d}\eta+\frac{\varepsilon}{\delta}\int_0^h\frac{\partial\sigma^{\alpha\beta}}{\partial\beta}\,\mathrm{d}\eta+\sigma^{\alpha\beta,\mathrm{S}}-\sigma^{\alpha\beta,\mathrm{B}}-\bar{k}\cdot\bar{t}_{\alpha}h. \tag{17}$$

- β Momentum

$$\delta\left[\frac{\partial(\bar{v}h)}{\partial t}+\frac{\partial(\bar{u}\bar{v}h)}{\partial\alpha}+\frac{\partial(\bar{v}^2h)}{\partial\beta}\right]=\varepsilon\int_0^h\frac{\partial\sigma^{\alpha\beta}}{\partial\alpha}d\eta+\frac{\varepsilon}{\delta}\int_0^h\frac{\partial\sigma^{\beta}}{\partial\beta}\,\mathrm{d}\eta+\sigma^{\beta\eta,\mathrm{S}}-\sigma^{\beta\eta,\mathrm{B}}-\bar{k}\cdot\bar{t}_{\beta}h. \tag{18}$$

- η Momentum

$$\chi_{\alpha}\lambda_{\alpha}\bar{u}^2(h-\eta)+\chi_{\beta}\lambda_{\beta}\delta^2\bar{v}^2(h-\eta)=\sigma^{\eta}(h)-\sigma^{\eta}(\eta)-(h-\eta)\bar{k}\cdot\bar{n}.$$

The distribution of σ^{η} along the depth is derived from this latter equation as

$$\sigma^{\eta}(\eta)=\sigma^{\eta,\mathrm{S}}-\left[\chi_{\alpha}\lambda_{\alpha}\bar{u}^2+\chi_{\beta}\lambda_{\beta}\delta^2\bar{v}^2+\bar{k}\cdot\bar{n}\right](h-\eta) \tag{19}$$

In these equations, the superscripts S and B indicate that the concerned variable is calculated at the free surface, S, or at the bed, B.

2.4. General depth integrated equations on an inclined and curved bed

Considering now the relationship between the dimensioned and dimensionless variables (10) the final equations in the dimensioned variables are:

Continuity

$$\frac{\partial(\bar{u}h)}{\partial\alpha}+\frac{\partial(\bar{v}h)}{\partial\beta}+\frac{\partial h}{\partial t}=0. \tag{20}$$

Momentum

- α Momentum

$$\rho\left[\frac{\partial(\bar{u}h)}{\partial t}+\frac{\partial(\bar{u}^2h)}{\partial\alpha}+\frac{\partial(\bar{u}\bar{v}h)}{\partial\beta}\right]=\int_0^h\frac{\partial\sigma^{\alpha}}{\partial\alpha}\,\mathrm{d}\eta+\int_0^h\frac{\partial\sigma^{\alpha\beta}}{\partial\beta}\,\mathrm{d}\eta+\sigma^{\alpha\beta,\mathrm{S}}-\sigma^{\alpha\beta,\mathrm{B}}-\rho gh\bar{k}\cdot\bar{t}_{\alpha}.$$

- β Momentum

$$\rho\left[\frac{\partial(\bar{v}h)}{\partial t}+\frac{\partial(\bar{u}\bar{v}h)}{\partial\alpha}+\frac{\partial(\bar{v}^2h)}{\partial\beta}\right]=\int_0^h\frac{\partial\sigma^{\alpha\beta}}{\partial\alpha}\,\mathrm{d}\eta+\int_0^h\frac{\partial\sigma^{\beta}}{\partial\beta}\,\mathrm{d}\eta+\sigma^{\beta\eta,\mathrm{S}}-\sigma^{\beta\eta,\mathrm{B}}-\rho gh\bar{k}\cdot\bar{t}_{\beta}.$$

- η Momentum

$$\sigma^{\eta}(\eta)=\sigma^{\eta,\mathrm{S}}-\rho\left[\chi_{\alpha}\bar{u}^2+\chi_{\beta}\bar{v}^2+g\bar{k}\cdot\bar{n}\right](h-\eta). \tag{21}$$

Applying the Leibniz's rule to the integrals of the derivatives of the stress tensor components results in the following alternative form of the α and β components of the momentum equations:

- α Momentum

$$\rho\left[\frac{\partial(\bar{u}h)}{\partial t}+\frac{\partial(\bar{u}^2h)}{\partial\alpha}+\frac{\partial(\bar{u}\bar{v}h)}{\partial\beta}\right]=\frac{\partial(\bar{\sigma}^{\alpha}h)}{\partial\alpha}+\frac{\partial(\bar{\sigma}^{\alpha\beta}h)}{\partial\beta}+f_R^{\alpha,\mathrm{S}}+f_R^{\alpha,\mathrm{B}}-\rho gh\bar{k}\cdot\bar{t}_{\alpha}. \tag{22}$$

- β Momentum

$$\rho\left[\frac{\partial(\bar{v}h)}{\partial t}+\frac{\partial(\bar{u}\bar{v}h)}{\partial\alpha}+\frac{\partial(\bar{v}^2h)}{\partial\beta}\right]=\frac{\partial(\bar{\sigma}^{\alpha\beta}h)}{\partial\alpha}+\frac{\partial(\bar{\sigma}^{\beta}h)}{\partial\beta}+f_R^{\beta,\mathrm{S}}+f_R^{\beta,\mathrm{B}}-\rho gh\bar{k}\cdot\bar{t}_{\beta}, \tag{23}$$

where

- $\bar{\sigma}^{ij}=\frac{1}{h}\int_0^h\sigma^{ij}\,\mathrm{d}\eta$

and the α and β components of the forces applied at the free surface, $\bar{f}_R^{\mathrm{S}}$, and at the bed, $\bar{f}_R^{\mathrm{B}}$, are obtained by applying the stress tensor to the normal to each surface

$$\bar{n}^{\mathrm{S}}=\left[-\frac{\partial h}{\partial\alpha},-\frac{\partial h}{\partial\beta},1\right],$$

$$\bar{n}^{\mathrm{B}}=[0,0,-1].$$

2.5. Fluid rheology

Considering a continuum sediment-fluid flow, Pierson and Costa [13] proposed a classification system of the gravity-driven flows based on the ranges of sediment concentration. In this system, the different types of flow are distinguished based on ranges of the sediment load and the rheological behavior.

A flow in which the sediment load is so low that it does not affect the flow behavior, or imparts no yield strength to the flow, is considered as normal streamflow. This may be the case of dam break problems where the fluid of concern is water and Newtonian rheology assumed for the fluid. As it is customary in shallow water problems, the viscous dissipation is neglected compared to the bed friction dissipation.

At the other side of the classification, granular flow occurs at high ranges of sediment concentration, where the mass loses its ability to liquefy, and frictional and collisional particle interactions dominate the flow behavior. The calculations performed by Savage and Hutter [17] on a series of experiments using a dry, granular, material indicate that the avalanche characteristics were fairly insensitivity to the material internal friction angle but more sensitive to the bed friction.

Therefore, for practical purposes the constitutive equation (4) for both type of flows may be reduced to

$$\boldsymbol{\sigma}=-p\mathbf{1}$$

and extended to intermediate flows from the point of view of the sediment load, the hyperconcentrated and debris flows, which are typically described using Bingham or Herschel–Bulkley rheologies.

Therefore,

$$-p(\eta)=\sigma^{\eta}(\eta)=\sigma^{\alpha}(\eta)=\sigma^{\beta}(\eta).$$

The distribution along the depth of the stress tensor is now calculated using Eq. (21). Considering, just for convenience, that the tractions at the free surface are zero, the depth averaged values is

$$\bar{p}=\frac{\bar{p}^{\mathrm{S}}+\bar{p}^{\mathrm{B}}}{2}=\rho\left[\chi_{\alpha}\bar{u}^2+\chi_{\beta}\bar{v}^2+g\bar{k}\cdot\bar{n}\right]\frac{h}{2}=\bar{\sigma}^{\alpha}=\bar{\sigma}^{\beta}.$$

It should be realized that the hydrostatic pressure distribution resulting in the case of the SWE incorporates now a centrifugal force term, proportional to χu^2.

Incorporating the value of the averaged normal stress components in (22) and (23) results in the final set of differential equations describing the flow of an spill of fluid on an inclined and curved bed

$$\frac{\partial h}{\partial t}+\frac{\partial(\bar{u}h)}{\partial\alpha}+\frac{\partial(\bar{v}h)}{\partial\beta}=0, \tag{24}$$

$$\frac{\partial(\bar{u}h)}{\partial t}+\frac{\partial(\bar{u}^2h)}{\partial\alpha}+\frac{\partial(\bar{u}\bar{v}h)}{\partial\beta}=-\frac{1}{2}\frac{\partial(\hat{g}h^2)}{\partial\alpha}+\frac{1}{\rho}f_R^{\alpha,\mathrm{B}}-gh\bar{k}\cdot\bar{t}_\alpha, \tag{25}$$

$$\frac{\partial(\bar{v}h)}{\partial t}+\frac{\partial(\bar{u}\bar{v}h)}{\partial\alpha}+\frac{\partial(\bar{v}^2h)}{\partial\beta}=-\frac{1}{2}\frac{\partial(\hat{g}h^2)}{\partial\beta}+\frac{1}{\rho}f_R^{\beta,\mathrm{B}}-gh\bar{k}\cdot\bar{t}_\beta, \tag{26}$$

where

$$\hat{g}=\chi_\alpha\bar{u}^2+\chi_\beta\bar{v}^2+g\bar{k}\cdot\bar{n}. \tag{27}$$

These equation can be written in compact form as

$$\frac{\partial}{\partial t}\begin{bmatrix}h\\ \bar{u}h\\ \bar{v}h\end{bmatrix}=\frac{\partial}{\partial\alpha}\begin{bmatrix}\bar{u}h\\ \bar{u}^2h+\frac{1}{2}\hat{g}h^2\\ \bar{u}\bar{v}h\end{bmatrix}+\frac{\partial}{\partial\beta}\begin{bmatrix}\bar{v}h\\ \bar{u}\bar{v}h\\ \bar{v}^2h+\frac{1}{2}\hat{g}h^2\end{bmatrix}=\begin{bmatrix}0\\ \frac{1}{\rho}f_{R,\alpha}^{\mathrm{B}}-gh\bar{k}\cdot\bar{t}_\alpha\\ \frac{1}{\rho}f_{R,\beta}^{\mathrm{B}}-gh\bar{k}\cdot\bar{t}_\beta\end{bmatrix} \tag{28}$$

and thus they can be cast in the conservation laws framework

$$\frac{\partial\boldsymbol{\phi}}{\partial t}+\frac{\partial\mathbf{F}_\alpha}{\partial\alpha}+\frac{\partial\mathbf{F}_\beta}{\partial\beta}=\mathbf{S}. \tag{29}$$

As regards the bed resistance force, $\bar{f}_R^{\mathrm{B}}$, there are a number of available descriptions, see for instance [4] for a compilation. The examples documented latter in this paper will consider the Chezy–Manning equation

$$\bar{f}_R^{\mathrm{B}}=-\frac{\rho g n^2|\bar{\mathbf{u}}|\bar{\mathbf{u}}}{h^{\frac{1}{3}}} \tag{30}$$

for Newtonian fluids and Coulomb friction for granular flows

$$\bar{f}_R^{\mathrm{B}}=-p^{\mathrm{B}}\tan\delta\frac{\bar{\mathbf{u}}}{|\bar{\mathbf{u}}|}, \tag{31}$$

where δ is the bed friction angle.

2.6. Comparison with the shallow water equations

Using the notation described in Fig. 1, the SWE are

$$\frac{\partial}{\partial t}\begin{bmatrix}h\\ \bar{u}h\\ \bar{v}h\end{bmatrix}+\frac{\partial}{\partial x}\begin{bmatrix}\bar{u}h\\ \bar{u}^2h+\frac{1}{2}gh^2\\ \bar{u}\bar{v}h\end{bmatrix}+\frac{\partial}{\partial y}\begin{bmatrix}\bar{v}h\\ \bar{u}\bar{v}h\\ \bar{v}^2h+\frac{1}{2}gh^2\end{bmatrix}=\begin{bmatrix}0\\ \frac{1}{\rho}f_{R,x}^{\mathrm{B}}-gh\frac{\partial Z}{\partial x}\\ \frac{1}{\rho}f_{R,y}^{\mathrm{B}}-gh\frac{\partial Z}{\partial y}\end{bmatrix}. \tag{32}$$

The parallelism between (28) and (32) is evident once $\partial Z/\partial x$ is recognized as $\bar{t}_\alpha \cdot \bar{n}$ and the centrifugal forces, proportional to χu^2, are incorporated into the body forces. However, it should be realized that this parallelism only exits when the curvilinear reference system used in the generalized description corresponds to the principal curvature directions.

3. Numerical model

There are a number of methods available to solve advection dominated problems as the one governed by Eq. (28). Within the FEM context, due to its accuracy and simplicity, the Two-step Taylor–Galerkin algorithm developed by Peraire [12] has been previously used by the authors to solve the SWE [9]. Considering the similarities pointed out in the previous section between the SWE equations (32) and their generalization for an inclined and curved bed, (28), the Two-step Taylor–Galerkin will be used to solve (28).

3.1. Two-step Taylor–Galerkin algorithm

The Two-step Taylor–Galerkin algorithm is widely used to solve advection dominated problems. Thus, references describing this algorithm and its numerical implementation abound. The interested reader is referred to [12,19] and references there in. For completeness, only an overview of the algorithm is included in the present paper.

The Taylor–Galerkin procedure for solving Eq. (29) starts from a second order expansion in time

$$\boldsymbol{\phi}^{n+1} = \boldsymbol{\phi}^n + \Delta t \left.\frac{\partial \boldsymbol{\phi}}{\partial t}\right|^n + \frac{1}{2}\Delta t^2 \left.\frac{\partial^2 \boldsymbol{\phi}}{\partial t^2}\right|^n, \tag{33}$$

where the first order time derivative of the unknowns can be calculated using Eq. (29)

$$\left.\frac{\partial \boldsymbol{\phi}}{\partial t}\right|^n = (S - \operatorname{div}\underline{F})^n.$$

To obtain the second order time derivative, the Two-step Taylor–Galerkin procedure considers an intermediate step between t^n and t^{n+1}. The aim of this first time step is to calculate the solution at a time $t^{n+1/2}$. This step is followed by a second one that brings the solution to t^{n+1}.

In this way, the first step results in

$$\boldsymbol{\phi}^{n+1/2} = \boldsymbol{\phi}^n + \frac{\Delta t}{2}(\mathbf{S} - \operatorname{div}\underline{F})^n \tag{34}$$

which allows the calculation of $\underline{\mathbf{F}}^{n+1/2}$ and $\mathbf{S}^{n+1/2}$.

Considering now a Taylor series expansion of the flux and source terms:

$$\underline{\mathbf{F}}^{n+1/2} = \underline{\mathbf{F}}^n + \left(\frac{\partial \underline{\mathbf{F}}}{\partial t}\right)^n \frac{\Delta t}{2},$$

$$\mathbf{S}^{n+1/2} = \mathbf{S}^n + \left(\frac{\partial \mathbf{S}}{\partial t}\right)^n \frac{\Delta t}{2}$$

and the values of $\underline{\mathbf{F}}^{n+1/2}$ and $\mathbf{S}^{n+1/2}$, the flux and sources time derivatives are calculated as

$$\left(\frac{\partial \underline{\mathbf{F}}}{\partial t}\right)^n = \frac{2}{\Delta t}\left(\underline{\mathbf{F}}^{n+1/2} - \underline{\mathbf{F}}^n\right),$$

$$\left(\frac{\partial \mathbf{S}}{\partial t}\right)^n = \frac{2}{\Delta t}\left(\mathbf{S}^{n+1/2} - \mathbf{S}^n\right).$$

Incorporating these expressions into the second order time derivative

$$\left.\frac{\partial^2 \boldsymbol{\phi}}{\partial t^2}\right|^n = \frac{\partial}{\partial t}(\mathbf{S} - \operatorname{div}\underline{F})^n$$

results in

$$\left.\frac{\partial^2 \boldsymbol{\phi}}{\partial t^2}\right|^n = \frac{2}{\Delta t}\left(\mathbf{S}^{n+1/2} - \mathbf{S}^n - \operatorname{div}\left(\underline{\mathbf{F}}^{n+1/2} - \underline{\mathbf{F}}^n\right)\right).$$

Now replacing the expressions for the first and second order time derivatives in the Taylor series expansion (33) allows the determination of the unknowns at time t^{n+1}

$$\boldsymbol{\phi}^{n+1} = \boldsymbol{\phi}^n + \Delta t\left(\mathbf{S}^{n+1/2} - \operatorname{div}\underline{\mathbf{F}}^{n+1/2}\right).$$

This equation is spatially discretized using conventional Galerkin weighting to finally result in the system of equations to be solved to obtain the unknown increments in the variables at the time step:

$$\underline{M}\Delta\phi = \Delta t\left(\int \underline{\mathbf{N}}\mathbf{S}^{n+1/2}\,\mathrm{d}\Omega - \int_{\Gamma_N} \underline{\mathbf{N}}\left(\underline{\mathbf{F}}^{n+1/2}\cdot\bar{n}\right)\mathrm{d}\gamma + \int \underline{\mathbf{F}}^{n+1/2}\operatorname{grad}\underline{\mathbf{N}}\,\mathrm{d}\Omega\right). \tag{35}$$

3.2. Algorithmic aspects

Due to the similarities between the generalized system of equations, (28), and the regular SWE, only small changes are necessary to adapt a code capable to solve the SWE for solving (28).

These changes consist in obtaining the curvilinear reference system and principal curvatures and to incorporate the appropriate stability requirements.

3.2.1. Calculation of the curvilinear reference system

The solution of the system of equations (28) requires the calculation of the curvilinear reference system and the curvatures in each point of the mesh. This can be done using standard equations from differential geometry of surfaces, see for instance [6]. However, they require the calculation of the second order spatial derivatives of the bed elevation, X_3.

This goal is achieved by calculating the first derivatives of the unknowns in the elements using the derivatives of the shape functions and from them, calculating the first derivatives in nodes using standard recovery techniques. From the first derivatives in nodes, second derivatives in elements are calculated in turn using the shape function derivatives and, using again nodal recovery techniques, the second derivatives in nodes.

There are a number of nodal recovery techniques available, see for instance [19]. As the examples presented in this paper use the three nodes triangles, the nodal averaging technique has been followed

$$\left(\int N^{\mathrm{T}}N\,\mathrm{d}\Omega\right)\bar{x} = \int N^{\mathrm{T}}x\,\mathrm{d}\Omega, \tag{36}$$

where
- N are the shape functions,
- $\bar{x}$ is the vector of nodal unknowns, first and second order derivatives, to be recovered and
- x is the value of the corresponding variable in each element in the mesh.

The right-hand side is evaluated by averaging the values calculated for the elements sharing the concerned node. Then, the system of equations can be solved iteratively using the lumped mass matrix, $\mathbf{M}_{\mathrm{L}}$, as the approximate inverse matrix of the consistent mass matrix, $\mathbf{M}_{\mathrm{C}}$, which is obtained by integrating the left-hand side of (36)

$$\bar{x}^{n+1} = \bar{x}^n + \mathbf{M}_{\mathrm{L}}^{-1}\left(\mathrm{RHS} - \mathbf{M}_{\mathrm{C}}\bar{x}^n\right).$$

For the calculation of the second derivatives of the bed elevation, using the lumped mass matrix, i.e., no iteration has been shown to be sufficient.

3.2.2. Drying and wetting areas

There are a number of possibilities to handle the issue of wetting and drying areas. The simple procedure to consider a null value for the variables corresponding to dry nodes in most cases is sufficient [9,14]. However, more accurate solutions as the proposed by Peraire [12] or that based on the level set technique from Sethian [16] can be used either for the SWE equations or for the generalized equations in the curvilinear reference system. No attempt has been pursued in the examples presented in this paper to use these more complex procedures and the former procedure, assigning null variables to dry nodes, has been used.

3.2.3. Time steps limitations

A linear advection problem with a source is represented by

$$\frac{\partial \phi}{\partial t} + A\frac{\partial \phi}{\partial x} = G\phi,$$

where A and G are constants.

For stability reasons, the numerical solution of this problem requires fulfillment of a condition on the Courant number, C,

$$C = \frac{A}{\frac{\Delta x}{\Delta t}} \leqslant \alpha$$

and on the source number, Sr,

$$\frac{C}{Sr} = G\Delta t \leqslant \alpha_1,$$

where
- $Sr = \frac{A}{G\Delta x}$,
- $\alpha = 1$ when using the lumped matrix and $\alpha = 1/\sqrt{3}$ when using the consistent mass matrix,
- $\alpha_1 = 2$ according to [12].

These conditions are applied to the SWE by diagonalization of the corresponding 1-D form of the equations, namely

$$\frac{\partial}{\partial t}\begin{bmatrix} 2c+u \\ 2c-u \end{bmatrix} + \begin{bmatrix} u+c & 0 \\ 0 & u-c \end{bmatrix}\frac{\partial}{\partial x}\begin{bmatrix} 2c+u \\ 2c-u \end{bmatrix} = \frac{1}{h}\begin{bmatrix} -f_{R,x} + gh\frac{\partial H}{\partial x} \\ f_{R,x} - gh\frac{\partial H}{\partial x} \end{bmatrix},$$

where

$$c = \sqrt{gh}$$

resulting

$$\Delta t \leqslant \min\left(\frac{\alpha\Delta x}{|u|+c}; \frac{\alpha_1 h}{\frac{|f_{R,x} - gh\frac{\partial Z}{\partial x}|}{2c-u}}\right).$$

The extension of these conditions to the 1-D generalized shallow water equations, (28),

$$\frac{\partial}{\partial t}\begin{bmatrix} h \\ uh \end{bmatrix} + \begin{bmatrix} 0 & 1 \\ -u^2 + \hat{g}h & 2u \end{bmatrix}\frac{\partial}{\partial \alpha}\begin{bmatrix} h \\ uh \end{bmatrix} = \frac{1}{h}\begin{bmatrix} 0 \\ \frac{1}{\rho}f_{R,\alpha} - gh\bar{k}\cdot\bar{t}_\alpha \end{bmatrix},$$

where $\hat{g}$ is given by Eq. (27), is straightforward as this system of equations can be written in terms of the Riemann's invariants as

$$\frac{\partial}{\partial t}\begin{bmatrix} 2\hat{c}+u \\ 2\hat{c}-u \end{bmatrix} + \begin{bmatrix} u+\hat{c} & 0 \\ 0 & u-\hat{c} \end{bmatrix}\frac{\partial}{\partial x}\begin{bmatrix} 2\hat{c}+u \\ 2\hat{c}-u \end{bmatrix} = \frac{1}{h}\begin{bmatrix} -\frac{1}{\rho}f_{R,\alpha} + gh\bar{k}\cdot\bar{t}_\alpha \\ \frac{1}{\rho}f_{R,\alpha} - gh\bar{k}\cdot\bar{t}_\alpha \end{bmatrix}.$$

Therefore, the time step should meet the following condition:

$$\Delta t \leqslant \min\left(\frac{\alpha\Delta x}{|u|+\hat{c}}; \frac{\alpha_1 h}{\frac{|\frac{1}{\rho}f_{R,\alpha} - gh\bar{k}\cdot\bar{t}_\alpha|}{2\hat{c}-u}}\right),$$

where $\hat{c} = \sqrt{\hat{g}h}$.

4. Numerical test cases

The test cases presented next check the effect of the bed slope and curvature on the main characteristics, i.e., depth and velocity, of a gravity-driven fluid flow. For this purpose, the test cases simulate the flow of fluids of different type onto a constant slope, 30%, chute connected to an horizontal runout surface by a circular arc section of 19 m radius, see Fig. 4. The fluid density is 2000 kg/m^3 and it is initially at rest. The flow is initiated by simulating an instantaneous removal of a retaining vertical wall 15 m height.

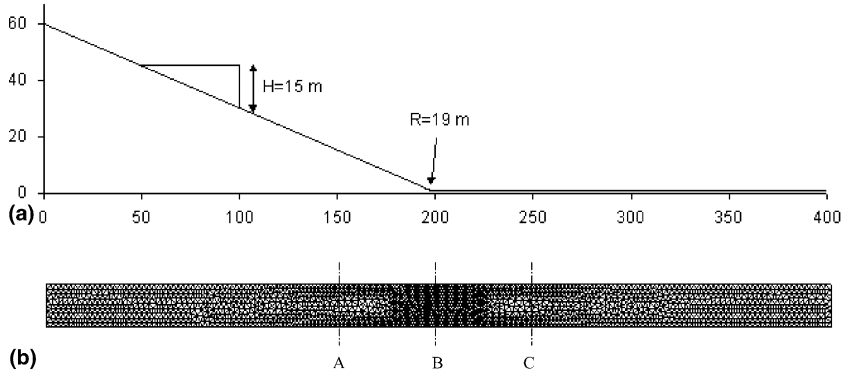

Fig. 4. Numerical test cases: (a) problem lay-out; (b) FEM mesh.

Fig. 4 also presents the mesh used in the spatial discretization. The mesh comprises 2081 nodes grouped in 3758 triangular elements; a finer mesh is used at the curved zone. Open boundary conditions are specified for all the problem boundaries.

The flow depth and velocity calculated by the proposed equations and the SWE are monitored at three control sections located as indicated in this figure.

4.1. Newtonian fluid

The first test case considers a Newtonian fluid. Therefore, according to Section 2.5, the bed friction is calculated using the Chezy–Manning equation, (30), considering the Manning resistance coefficient of many typical applications, 0.01.

As expected, the evolution of the flow depth calculated at the control section A, located at the chute before the curved section, is practically indistinguishable of whether or not the curvature effects are incorporated in the problem formulation. However, the same observation is made at control section C, located at the runout surface beyond the curved section. Finally, as regards control section B located in the curved section, a reduced effect is observed in the depth evolution, see Fig. 5: the evolution is quite similar with a difference in the peak value of just 0.2 m.

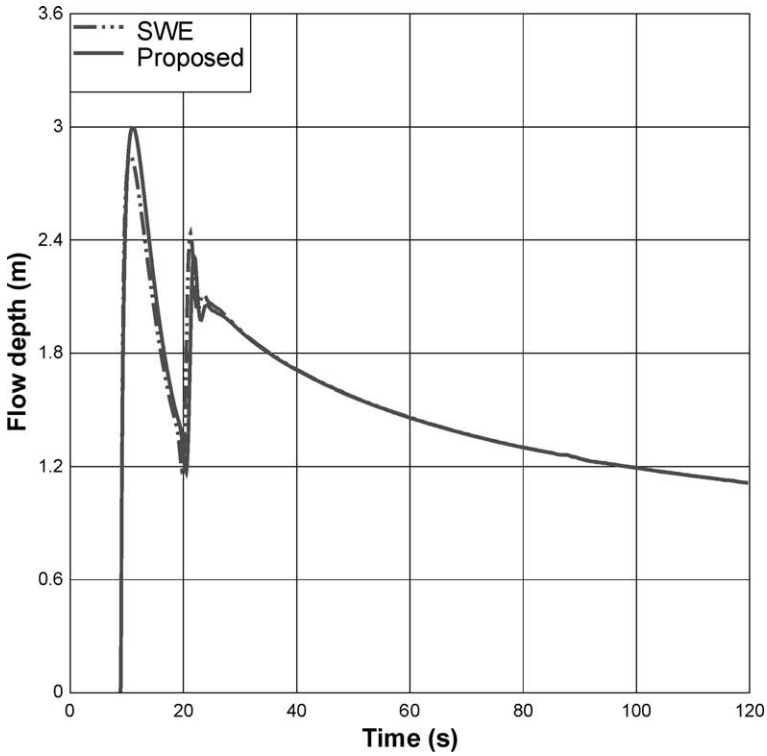

Fig. 5. Evolution of the flow depth at control section B. Newtonian fluid.

4.2. Granular flow

The second test case involves a granular flow. Thus, according to Section 2.5, the bed resistance force is calculated using Coulomb friction, Eq. (31). This test case considers a bed friction angle of 10°, slightly lower than the bed slope angle of 16°.

As regards the evolution of the flow depth at control section A, the results are, as expected, independent of the problem formulation and at control section B the differences remain reduced as for the Newtonian fluid case.

However, there is a significant difference in the flow depth calculated at point C, located at the runout surface. In effect, either the peak value and the evolution are different, as depicted in Fig. 6. Besides, the stoppage distance of the rear of the pile is 206 m when considering the effect of curvature and 212.5 m when ignored. Finally, there is another effect on the pile dimensions: the length of the pile is 4.5 m longer when the curvature effects are ignored and its height is consequently decreased.

At control section B the evolution of the flow velocity calculated by both formulations is equivalent although slightly lower velocities, by 1 m/s, are calculated when the curvature effects are incorporated in the problem formulation. At control section C, as expected from the depth history, the evolution of the flow velocities is quite different, see Fig. 7.

These effects are attributed to the enhanced bed friction in the arc section motivated by the curvature effect, a centrifugal force, that raises the normal stress at the bed and, thus, the energy loses due to the enhanced Coulomb type friction.

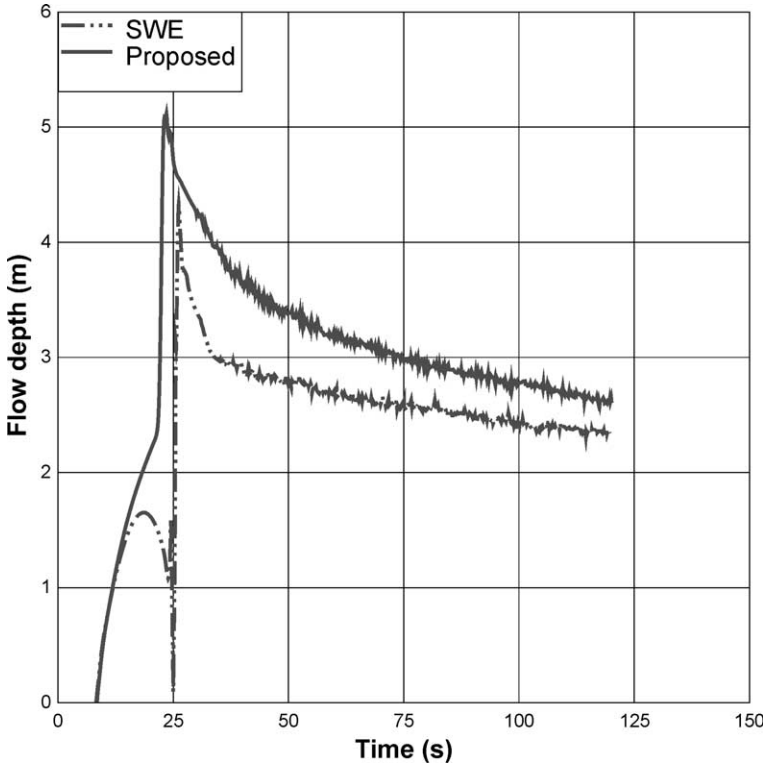

Fig. 6. Evolution of the flow depth at control section C. Granular flow.

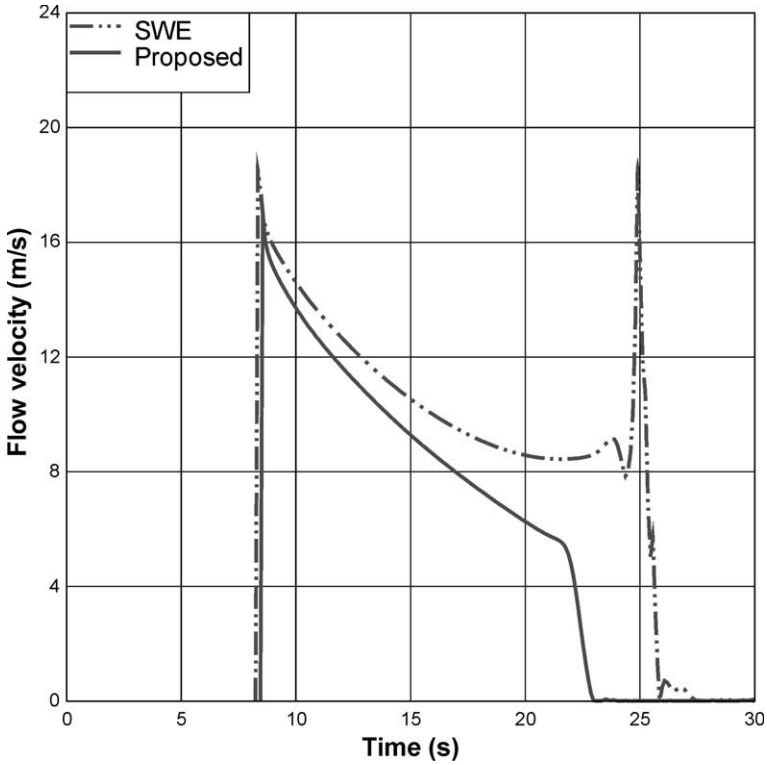

Fig. 7. Comparison of the evolution of the flow velocity calculated at control section C.

5. Conclusions

The derivation of Shallow Water Equations considers a reference system where gravity is approximately perpendicular to the free surface and to the bed. In this way, the fluid velocities should be quasi-horizontal. This assumption places restrictions to the application of SWE to the analysis of gravity-driven fluid flow problems in steep slopes or topographies including changes in the slopes, that had not been previously quantified.

To overcome these restrictions, the gravity-driven flow of a general fluid has been described in this paper using depth integrated equations which incorporates steep slopes and curvature effects. Although the derivation is somewhat lengthy, the resulting equations are simple when using the principal curvature directions in each point as the curvilinear reference system. The generalized equations are applicable for any slope and the only assumption made is that the fluid flow depth is small compared to typical dimensions of the fluid spill and to the radius of curvature.

Due to the similarities between these Generalized Shallow Water Equations and the Shallow Water Equations, the numerical methods used to solve the latter are directly applicable to the solution of the GSWE. The application basically requires the calculation of the curvilinear reference system and curvatures in each node and element of the mesh. This calculation is done before the time integration of the equations.

The results of the numerical test cases indicate that the SWE provides with solutions that are quite closed to the results using the generalized formulation here proposed when the bed friction law does not depend on the normal stress at the bed. Therefore, in this case there is no need to incorporate the centrifugal forces due to curvature into the momentum conservation equations. In the case the bed friction depends on the normal

stress, the centrifugal forces due to curvature increases the normal stress at the bed and the corresponding energy dissipation by friction significantly affects the fluid flow characteristics.

References

[1] M. Abbott, Computational Hydraulics. Elements of the Theory of Free Surface Flows, Pitman, London, 1979.
[2] F. Alcrudo, P. García-Navarro, A high resolution Godunov-type scheme in finite volume for the shallow water equations, Int. J. Numer. Meth. Fluids 16 (1991) 489–505.
[3] G.B. Whitham, Linear and Nonlinear Waves, Wiley, New York, 1974.
[4] O. Hungr, A model for the runout analysis of rapid flow slides, debris flows, and avalanches, Can. Geotech. J. 32 (1995) 610–623.
[5] R. Iverson, R. Denlinger, Flow of variably fluidized granular masses across three-dimensional terrain. Coulomb mixture theory, J. Geophys. Res. 106 (Bl) (2001) 537–552.
[6] J.-L. Batoz, G. Dhatt, Modelization Des Structures Par Elements Finis, vol. 3, Hermés, 1992.
[7] J.M.N.T. Gray, M. Wieland, K. Hutter, Gravity-driven free surface flow of granular avalanches over complex basal topography, Proc. R. Soc. Lond. 455 (1999) 1841–1874.
[8] M. Quecedo, M. Pastor, Application of the level set method to the finite element solution of two-phase flows, Int. J. Num. Meth. Eng. 50 (2001) 645–663.
[9] M. Quecedo, M. Pastor, A reappraisal of Taylor–Galerkin algorithm for drying–wetting areas in shallow water computations, Int. J. Numer. Meth. Fluids 38 (2002) 515–531.
[10] M. Sussman, P. Smereka, S. Osher, A level set approach for computing solutions to incompressible two-phase flow, J. Comput. Phys. 114 (1994) 146–159.
[11] L. Malvern, Introduction to the Mechanics of a Continuous Medium, Prentice-Hall, Englewood Cliffs, NJ, 1969.
[12] J. Peraire, A finite element method for convection dominated flows, Ph.D. Thesis, University of Wales, Swansea, 1986.
[13] T. Pierson, J. Costa, A rheologic classification of subaerial sediment-water flows, Rew. Eng. Geol. VII (1987) 1–12.
[14] J.S. Vincent, P. Bonneton, Numerical modelling of bore propagation and run-up on sloping beaches using a MacCormack TVD scheme, J. Hydraulic Res. 39 (2001) 41–49.
[15] S.B. Savage, K. Hutter, The motion of a finite mass of granular material down a rough incline, J. Fluid Mech. 199 (1989) 177–215.
[16] J. Sethian, Level Set Methods. Evolving Interfaces in Geometry, Fluid Mechanics, Computer Vision, and Material Science, Cambridge University Press, Cambridge, 1996.
[17] S.V. Savage, K. Hutter, The dynamics of avalanches of granukar materials from initiation to runout, Acta Mechanica 86 (1991) 201–223.
[18] E. Toro, Shock-Capturing Methods for Free-Surface Flows, Wiley, New York, 2001.
[19] O. Zienkiewicz, R. Taylor, The Finite Element Method, Butterworth-Heinemann, 2000.